Atmospheric correction for inland waters. Application to SeaWiFS and MERIS.

Jérome Vidot*[a] and Richard Santer**[a]

[a] ELICO, UMR CNRS 8013; Université du Littoral Côte d'Opale (France)

ABSTRACT

As the spatial resolution is improved for "ocean colour" satellite sensors, such observations become relevant to monitor water quality for lakes. The required atmospheric corrections can not be conducted using the standard algorithms developed for ocean: need to account for the lake elevation, high water turbidity… The new generation of sensors has more spectral bands which allow to characterize the aerosol over dark land pixels (vegetation in the blue and in the red). Dense vegetation is identified using a spectral index and its reflectance is known from auxiliary data. We then derive, from the top of atmosphere radiances in two spectral bands, the optical thickness and the size distribution for aerosol. Knowing the aerosol model in the lake vicinity, it is then possible to apply atmospheric corrections over inland waters. A specific difficulty arises from the contamination of the photons reflected by the surrounding land and scattered towards the sensor. A simple formulation to correct this adjacency effect can be used for the Rayleigh scattering. We force the 865 nm water reflectance to be equal to zero to derive for each water pixel a function describing the aerosol adjacency effect. Assuming that the aerosol phase function does not vary much with the wavelength, we can correct all the spectral bands. The different stages of this new algorithm are illustrated on SeaWiFS.

1. ATMOSPHERIC CORRECTION: CURRENT STATUS FOR ALGORITHMS OVER OCEAN AND LIMITATIONS FOR INLAND WATERS.

All atmospheric correction algorithms over ocean are made to get the water leaving radiances over the sea level from the total radiances recorded at the top of the atmosphere. The water leaving radiances are thus made of photons that have crossed the atmosphere down to the ocean, and then have twice crossed the air-surface interface before reaching the sensor after a second atmospheric travel. These quantities carry information about the bio-optical state of the oceans upper layer, which is of great importance for bio-geochemical studies of the ocean (Antoine and Morel, 1998).

But to get a better accurate water leaving radiances we need to make correction of the possible photons that have reached the sensor without interaction with bio-optical media. These photons can have different origins, scattered from molecules and aerosols of the atmosphere or reflected from the surface surrounding the target. Some of these phenomena are taken into account in atmospheric correction algorithms over ocean. But there are some limitations of these algorithms over turbid waters or coastal waters. The basic concept of retrieval of water leaving radiances is the darkness of water in the near infra red (700-900 nm), so the measured radiances on this spectral range comes from the atmosphere. From these radiances, we obtain the physical characteristics of aerosols and molecules and we are able to make corrections.

The limitations of these algorithms for turbid waters come from different origins. The first one is the assumption of zero water leaving radiance in the near infrared. This assumption is invalid because lake waters are not dark in the red.

The second one comes from the molecular correction. For corrections over ocean, the surface pressure is taken on the sea surface. But for lakes, this surface pressure depends on the altitude of the lake. The last problem concerns the standard aerosol models used. These models are realistic for open oceans but are may be not over coastal and inland waters.

For example, we applied the Gordon and Wang algorithm (Gordon, 1997) on SeaWiFS scene of the Balaton Lake (47° N, 17°50' E). The size of the lake is about 70 km*15 km which is representative of a large European lake. On september, 21th, 1998, we applied the GW algorithm and we reported, in figure 1, the aerosol optical thickness (OAT). AOT appears quite scattered with larger values at the edge of the lake up to 0.3 while the mean value is 0.12. In the middle of the lake, we reported for two different pixels the water reflectance for all the SeaWiFS bands (Figure 2). We

Ocean Remote Sensing and Applications, Robert J. Frouin, Yeli Yuan, Hiroshi Kawamura, Editors, Proceedings of SPIE Vol. 4892 (2003) © 2003 SPIE · 0277-786X/03/$15.00

can see that the algorithm falls in the blue bands giving negative values. The atmospheric correction is overestimated because the AOT also was.

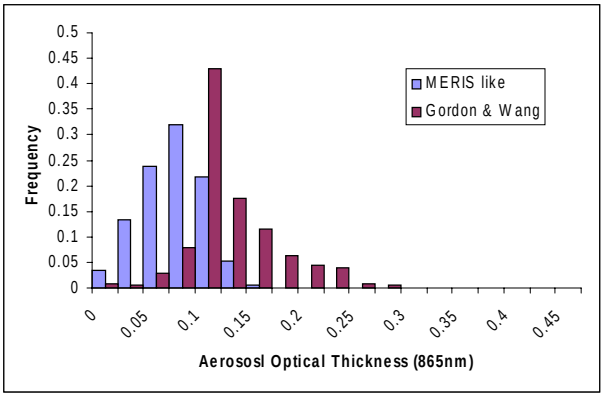

Fig. 1: Histogram of the AOT at 865 nm as obtained by the GW algorithm over the Balaton lake.

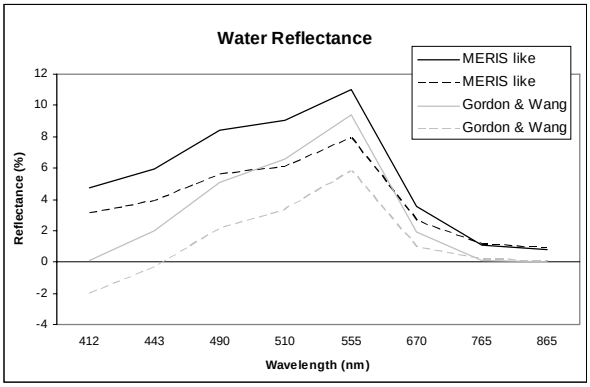

Fig. 2: Water reflectance spectra obtain for two points in the middle of the lake by the GW algorithm.

2. ATMOSPHERIC CORRECTIONS OVER LAND. THE MERIS-LIKE ALGORITHM

2.1 Formulation of the signal

General principle of atmospheric correction process is mainly based on the scheme developed for MERIS (Santer *et al.*, 1999; Ramon and Santer, 2001). The first step is applied to the top of atmosphere (TOA) reflectance for the correction of gaseous transmission, especially ozone and water vapour. ρ_{ng} is the reflectance signal ignoring the gaseous absorption and T_g the gaseous transmittance, which can be evaluated from simulations of radiative transfer model. In practice, this gaseous correction concerns the ozone in the Chapuis band and some residual water vapour absorption in the red and near infrared.

The second correction is done for the Rayleigh molecular scattering effect. Schematically, the remaining signal ρ_{ng} is both constituted by a Rayleigh part ρ_R and an aerosol plus ground part T_R. ρ_{ag}, where T_R is the Rayleigh transmittance and ρ_{ag} the signal of both aerosol layer and ground surface. T_R and ρ_R are evaluated from simulations of radiative transfer model, as a function of the surface pressure and the geometrical conditions. Surface pressure and thus Rayleigh vertical optical thickness is derived from the barometric pressure at sea level. A digital elevation map (DEM) has to be used to correct for the site elevation.

For the correction of the signal of the aerosol impact, knowledge of aerosol type and aerosol optical thickness are needed. The aerosol type is determined over dense dark vegetation (DDV) pixels, where the ground reflectance is supposed to be known. Applying the same principle than above, and knowing the aerosol reflectance ρ_a and aerosol transmittance T_a from simulations of radiative transfer model, the ground surface reflectance ρ_g can be easily calculated from the formula :

$$\rho_{aG} = \rho_a + T_a(\mu_s)\frac{\rho_G}{1-\rho_G S_a}T_a(\mu_v) \qquad (1)$$

where ρ_a, T_a and S_a are respectively the intrinsic reflectance, the transmittance and the spherical albedo relative to the aerosols, ρ_{ag} is the aerosol-ground contribution, ρ_G is the surface reflectance, μ_s and μ_v are the cosine of sun's angle θ_s and view's angle θ_v, respectively. The denominator of Eq. (1) accounts for the multiple interactions between the atmosphere and the surface.

From the blue and red top of aerosol reflectances, we can just expect to derive two informations on the aerosol model such as the abundance on the atmospheric column, (or the aerosol optical thickness) and a parameter for the size

distribution. Due to poor knowledge of aerosols, the simplest but realistic description for the size distribution by a power law is assumed :

$$n(r) = r^{\alpha-3} \tag{2}$$

where the Angström coefficient α (Junge, 1963) describes the wavelength dependency of the aerosol optical thickness τ_a :

$$\frac{\tau_a(\lambda)}{\tau_a(\lambda')} = \left(\frac{\lambda}{\lambda'}\right)^{\alpha} \tag{3}$$

Assuming a Junge power law, the phase matrix does not depend on wavelength, and the main parameter is the phase function. We generated phase functions into look up tables (LUTs) for the aerosol models and 83 scattering angles. Thus, for a given aerosol model, we just need to model the dependence in τ_a. The computation of the aerosol reflectance is based on the same idea as the Rayleigh reflectance, e.g. de-coupling primary and multiple scattering and using a Fourier series expansion. The total transmission T_a, for the direct to direct path, is equal to $T_a(\theta_s).T_a(\theta_v)$. For each aerosol model, we can extract $T_a(\theta)$ from LUTs built with 6S radiative transfer code, for 12 zenith angles and 15 values of τ_a.

2.2 Aerosol remote sensing over DDV

The usual strategy for the remote sensing of aerosol over land is based on the use of dark targets (Kaufman *et al.*, 1997 ; Kaufman and Sendra, 1988). At first, the aerosol retrieval over dark target was based on the detection of green forests (dark pixels) using the Normalized Difference Vegetation Index NDVI (Tucker, 1979) and the near-IR reflectance. The dark vegetation was determined by high values of NDVI with low reflectance in the near-IR. DDV is dark in the spectral bands where the chlorophyll absorption is strong, in the blue and in the red. These bands are always present in ocean colour mission. We will use here on the possibility to detect the DDV surfaces based on ARVI (Kaufman and Tanré, 1992) which uses the channels in the blue, red and near-infrared. The ARVI is defined as follows :

$$ARVI = \frac{\rho_{NIR} - (\rho_r - \gamma(\rho_b - \rho_r)}{\rho_{NIR} + (\rho_r - \gamma(\rho_b - \rho_r)} \tag{4}$$

where ρ_b, ρ_r and ρ_{NIR} are reflectances, corrected for molecular scattering and gaseous absorption, observed respectively in the blue, red and near infrared channels (for MERIS, 443nm, 670nm and 865nm). A value of γ close to 1.3 corresponds to dark dense forests (Santer *et al.*, 1999). A pixel is identified as dark vegetation when its ARVI is greater than an ARVI threshold. The thresholds are computed versus geolocation and geometry for a set of DDV BRDF models described in the next section. It is also assumed that the aerosols are continental and the horizontal visibility is 23 km.

Once DDV surfaces are identified, we can retrieve aerosol properties assuming a standard value for the DDV reflectances. We use the DDV models proposed by Leroy *et al.* (1998) from POLDER data. During January and June 1997, the clearest days have been selected using the POLDER aerosol product. Because the aerosol loading was small, the classical NDVI has been initially used to identify DDV occurrences. The viewing capabilities of POLDER allow covering 12 view angles and the sun zenith angle varies along the track. A canopy transfer model is used to fit the data and allows extending the determination of the bi-directional reflectances to a large range of angles. The latter study gives DDV reflectances LUTs versus the solar angle, for the standard models.

The aerosol path radiance can be retrieved in two spectral bands over DDV. From these two information, we can get two parameters on the aerosols : the Angström coefficient α and the aerosol optical thickness τ_a at 550 nm. The aerosol refractive index m has to be specified by the user with a default option m=1.45. The aerosol scaterring functions ρ_a, T_a, S_a are precomputed for three refractive indices : 1.33, 1.45 and 1.55 ; for 4 values of α ranging between 0 and 1.5 ; for 16 values of τ_a at 865 nm between 0 and 1.5. For more detailed informations about the remote sensing of aerosol over land from MOS see: Santer *et al.*, 1999 and Ramon and Santer, 2001. The validation of the algorithm products has also

been done, (Schmechtig *et al.*, 2001), comparing retrieved aerosol products with *in situ* sunphotometer measurements of the AErosol RObotic NETwork (AERONET) (Holben *et al.*, 1998).

3. ATMOSPHERIC CORRECTION OVER INLAND WATERS.

3.1 To apply the land algorithm to retrieve the water leaving radiance

The MERIS-like land algorithm was applied to SeaWiFS scenes collected during July and August of the year 1998 over the Balaton Lake. The lake is surrounded by forests and a substantial number of DDV pixels were selected. For the scene on 07/21/1998, the aerosol optical thickness at 865 nm was 0.091 and represents standard conditions. The OAT retrieved by the Meris-like algorithm, figure 1, are less scattered than with the GW algorithm despite the fact that it correspond to a larger area around the lake. Table 1 summarizes the outputs of the aerosol remote sensing around the Balaton lake during 1998 with a representative range of OAT between a very clear day (Julian day 211) and a quite turbid one (day 216).

julian day	θs	θv	Δφ	Θ	χ	DDV (%)	<α>	<τa(865)>	ρ_F (%)
211	30	34	41	158	60	6,21	0,5	0,011	1,75
213	30	26	25	168	55	3,05	-0,47	0,159	6,82
214	34	60	56	133	82	0,42	-0,04	0,467	9,85
215	30	22	8	171	52	2,17	-0,35	0,16	6,03
216	33	55	56	137	77	0,6	-0,35	0,437	9,2
218	33	48	54	143	71	5,5	-0,16	0,156	20,89
219	31	35	52	152	59	6,33	-0,48	0,094	11,05
220	33	40	50	150	65	4,31	-0,42	0,107	8,33
221	31	44	60	143	64	4,34	-0,14	0,137	15,5
222	33	32	40	159	61	4,33	-0,44	0,089	3,94
223	37	63	58	130	86	1,2	0,21	0,189	9,93
224	33	25	19	168	57	2,24	-0,44	0,124	6,01

Table 1: General conditions of observations and results of the MERIS-like algorithm: percent DDV pixel, α and AOT at 865 nm. Last column is the relative contribution at 865 nm of third Fresnel reflection.

Surface reflectance at 865 nm and 670 nm are displayed in Figure 3 for the 21 September, 1998. First of all, the water reflectance at 865 nm is as expected close to zero. That's mainly occurs in the middle of the lake. The land is very bright at 865 nm; we will address later the problem of the adjacency effect which arises when the contrast between land and water is high. At 670 nm, the DDV pixels present typical reflectances of around 2.5 percent. We can see on this image the spatial distribution of the DDV pixels around the lake. The lake reflectance at 665 nm is very similar to the DDV reflectance at this wavelength. Also, for two pixels in the middle of the lake, we reported in Figure 2, the water reflectance for all the SeaWiFS bands. Compared to GW outputs, the water reflectances have a better geophysical meaning with a spectral signature representative of inland waters.

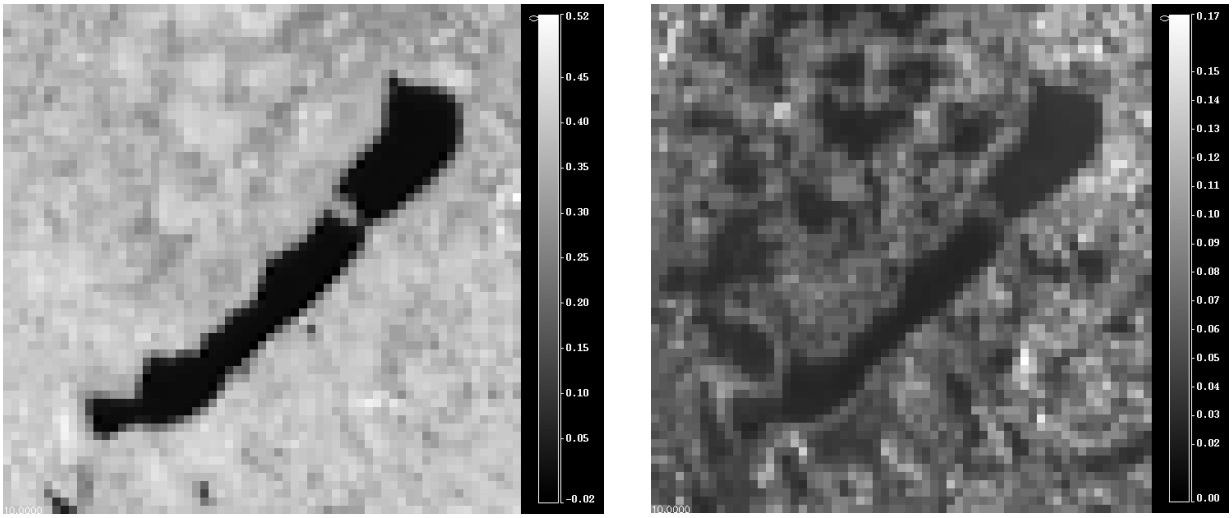

Fig. 3: water reflectances in the Balaton Lake as measured by SeaWiFS at 865 nm (left) and 670 nm (right) and atmospherically corrected by the MERIS-like algorithm

3.2 Correction from the Fresnel reflection

Fig. 4: Schematic representation of the Fresnel reflection (left) and of the adjacency effect (right)

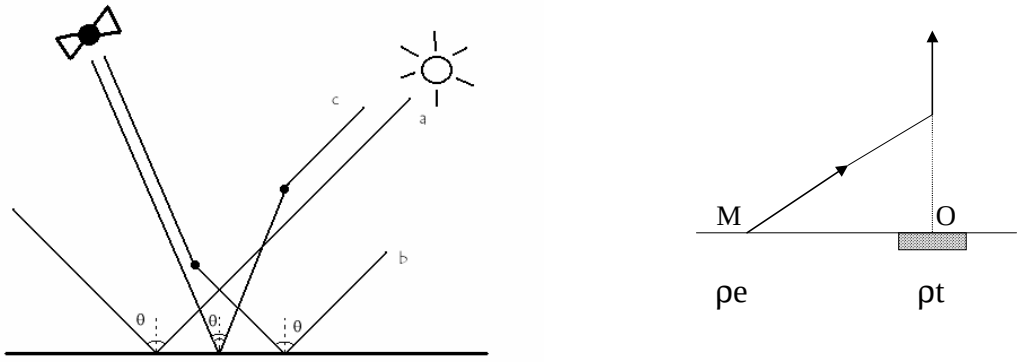

Even in the middle of the lake, the water is not strictly dark (see figure 2). This is may be due first to the accuracy of the atmospheric correction. Also, over water exists a non-negligible coupling term between the atmospheric scattering (mostly the aerosol forward scattering) and the Fresnel reflection. Figure 4, left, illustrates this coupling for a flat water surface (mirror) assuming the primary scattering approximation for the coupling between scattering and reflection. The atmospheric path radiance computed over a dark target L_{atm} has to be corrected taking into account the Fresnel reflection. The direct to direct reflection (a) corresponds to the sun glint. This geometry is useless for water colour analysis and actually avoids by SeaWiFS thanks to the instrument tilt of 25°. If we are not in the sun glint spot, the reflected solar beam scattered then to the sensor (b) does not exist on small lakes because the Fresnel reflection does not occurs over the surrounding land. We just have the downwelling radiance reflected towards the sensor (c). In a first approximation, this term can be express as:

$$dL_{atm} = \tau \frac{p(\chi)}{4\mu_v} r(\theta_v) \tag{5}$$

Where, the scattering angle χ corresponding to this forward scattering is given by:

$$\cos(\chi) = \cos(\theta_v)\cos(\theta_s) - \sin(\theta_s)\sin(\theta_v)\cos(\varphi) \tag{6}$$

θ_v is the view zenith angle, θ_s is the sun zenith angle and φ is the azimuth difference :

$$p(\chi) = \frac{p_a(\chi)\tau_a + p_m(\chi)\tau_m}{\tau_a + \tau_m} \tag{7}$$

Subscript *a* and *m* corresponds respectively to aerosols and molecules.
In equation (5), the Fresnel coefficient *r* is computed for the view angle θ_v, *p* is the aerosol phase function computed for the forward scattering angle χ.
Assuming that $L^{(0)}_{atm}$ is the radiance if the target is black. $L^{(0)}_{atm}$ can be expressed using the same approximation than in equation (5) as:

$$L^{(0)}_{atm} = \tau \frac{p(\theta)}{4\mu_v} \tag{8}$$

Where

$$\cos(\theta) = -\cos(\theta_v)\cos(\theta_s) - \sin(\theta_s)\sin(\theta_v)\cos(\varphi) \tag{9}$$

The atmospheric path radiance, accounting for the Fresnel reflection, is:

$$L_{atm} = L^{(0)}_{atm} + dL_{atm} = L^{(0)}_{atm}\left[1 + \frac{p(\chi)}{p(\theta)} r(\theta_v)\right] \tag{10}$$

To remove the time variation of incident direct solar irradiance, we refer to reflectance instead of radiance. So the equation (10) becomes :

$$\rho_{atm} = \rho^{(0)}_{atm}\left[1 + \frac{p(\chi)}{p(\theta)} r(\theta_v)\right] = \rho^{(0)}_{atm} + \rho_F \tag{11}$$

Where,

$$\rho_F = \rho^{(0)}_{atm} \frac{p(\chi)}{p(\theta)} r(\theta_v) \tag{12}$$

For the series of images atmospherically corrected, we illustrated this Fresnel correction giving and the relative importance of this correction at 865 nm compared to the removal of the atmospheric path radiance Table 1. The series of lake images is then corrected from the Fresnel contribution, but it does not change the shape of the surface reflectance spectra.

3.3 Modeling of the adjacency effects

By atmospheric scattering, a fraction of the incoming signal can originate from the neighbourhood of the target (Santer and Schmechtig, 2000). The effect results on photons reflected by the environment. If the surface is assumed to be spatially homogeneous, the 6S code proposes to formulate the contribution of the surface to the adjacency effects can be expressed as:

$$\rho^*_t = T(\mu_S)T(\mu_V)\left[\frac{\rho_G}{1 - \rho_G s}\right] \tag{13}$$

Where T is the total transmittance (the total downward irradiance, direct and diffuse, at the surface level for a black surface, normalized by the direct solar irradiance at the top of the atmosphere), ρ_t is the surface reflectance and s is the spherical albedo of the atmosphere.
If the surface is not homogeneous (Figure 4, right), the reflectance ρ_t, at a given point M, directly observed from the sensor, generally differs from the reflectance ρ_e of the surroundings. This contribution to the effect to the surface can be expressed as :

$$\rho_t^* = \left[\rho_t \exp\left(\frac{-\tau}{\mu_v} \right) + \langle \rho \rangle t_d(\mu_v) \right] \left[\frac{T(\mu_s)}{1 - \langle \rho \rangle s} \right] \tag{14}$$

Where τ is the total aerosol optical thickness, t_d is the diffuse transmittance, and $<\rho>$ is an average reflectance.
The adjacency effect increases with the atmospheric scattering (which is more effective at short wavelengths) but also with the contrast between land and water (Lyapustin and Kaufman, 2001). The additional surface reflectance $\Delta\rho^*$ (following Eqs. (13) and (14)) due to the adjacency effect brings on the photons reflected by the ground and scattered towards the sensor with :

$$\Delta\rho^* = T(\mu_s)(\rho_t - \langle \rho \rangle) t_d(\mu_v) \tag{15}$$

For a nadir view, the location of M is expressed in polar coordinate (r,ϕ), and we expressed $<\rho>$ as:

$$\langle \rho \rangle = \int_0^\infty \rho(r) g(r) dr \tag{16}$$

In which,

$$\rho(r) = (1/2\pi) \int_0^{2\pi} \rho(r,\varphi) d\varphi \tag{17}$$

Is the average azimuth value of the surface reflectance. If the location of M is given in Cartesian coordinates, then:

$$< \rho >= \int_{-\infty}^{\infty} \int_{-\infty}^{\infty} g(x,y) \rho(x,y) dx dy \tag{18}$$

in which $g(x,y)$, usually called in the literature the atmospheric point spread function (psf), (see for example Vermote *et al.*, 1995), corresponds to the fraction of incident photons reflected in M by a lambertian reflector of unit reflectance and then scattered towards the sensor. To evaluate theoretically the psf, the Monte Carlo method is used to solve the transfer equation in the backward mode.
A simple modelling of the adjacency effects is proposed in the 6S code for a nadir view and for a scene corresponding to a uniform disk (radius R) of reflectance ρ_t, surrounded by a uniform infinite surface of reflectance ρ_e with:

$$\langle \rho \rangle = \rho_t F(R) + \rho_e (1 - F(R)) \tag{19}$$

$F(R)$ is simply the integral of $r*g(r)$ between 0 and R. This function is modelled (or analytically expressed) from a best fit of Monte Carlo simulated data both for the Rayleigh and for the aerosols. Rayleigh scattering and aerosol scattering are de-coupled. $F(R)$ gives the relative contribution to $<\rho>$ of surface points not farther than a distance r apart from the origin. So $F(R)$ is expressed as:

$$F(R) = 2\pi \int_0^R r g(r) dr \tag{20}$$

3.4 Correction of the adjacency effects by the molecules

For molecules, an analytical formulation of F(R) is available with:

$$F_m(R) = a_m \exp(-\alpha_m R) + b_m \exp(-\beta_m R) \tag{21}$$

With a_m = 0.93, b_m= 0.07, α_m= 0.08, β_m= 1.1
Following the Eq. (15), the Rayleigh scattering due to the environment is:

$$\Delta\rho_m^* = T(\mu_s)(\rho_t - \langle\rho_m\rangle)t_d^m(\mu_v) \tag{22}$$

For the application of the Rayleigh scattering due to the environment on the series of images of the Balaton Lake, we applied the Eq. (14) on inland water pixels so we calculate <ρ> with :

$$\langle\rho_m\rangle = \Delta S\left[\sum_{i=1}^{n}\sum_{j=1}^{n} g(i,j)\rho(i,j)\right] \tag{23}$$

Where,

$$\begin{cases} g(r) = (1/2\pi r)\dfrac{\partial F(r)}{\partial r} \\ r = \sqrt{(i^2 + j^2)} \end{cases} \tag{24}$$

ΔS represent the surface of a pixel, *(i,j)* the coordinates of the pixel and *n* the size of the sub-window where the Rayleigh scattering is effective. Typically, this effect spread to 10 Km around, so we applied the calculation on a sub-window of 10*10 pixels around each inland water pixels. All Balaton lake scenes have corrected from this effect.

3.5 Correction of the adjacency effects by the aerosols.

The surface reflectance at 865 nm shows large differences in reflectance between water and land. A histogram of the scene indicates that the land reflectance is well peaked around 0.4 while the water is dark. To correct the adjacency effect by the aerosols, we use the same equations as Eq. (22) for the molecules. So, this equation is expressed as

$$\Delta\rho_a^* = T(\mu_s)(\rho_t - \langle\rho_a\rangle)t_d^a(\mu_v) \tag{25}$$

In Eq. (25), the dependence of the correction to the OAT is given in the atmospheric transmittances: direct T for the downward or diffuse t for the upward. The remaining, proportional to the land-water contrast, describes the scattering properties of the aerosols and can be expressed as:

$$\langle\rho_a\rangle - \rho_t = f_a(\rho_e - \rho_t) \tag{26}$$

If the land-water contrast strongly depends upon the wavelength, the aerosol scattering described in Eq. (26) by the function f_a does not depends munch on λ. This is strictly the case for the Junge size distribution we selected.
To calculate the function f_a, we made the assumption that the water is black on the near infrared wavelength at 865 nm for SeaWiFS. This assumption is always valid except for very high turbidity (more then 50 mg/l). So Eq. (26) becomes

$$\langle\rho_a\rangle = f_a\overline{\rho_e} \tag{27}$$

The last term of the equation is the average land reflectance around the lake. That does not mean that the land is homogeneous but that at a given distant d for the considered water pixel, we can assumed that the averaged value of the land reflectance is constant irregardless of d. $<\rho_a>$ is the water reflectance corrected from the Fresnel reflectance and the molecular scattering due to the environment. For each pixel of the lake, we derived the function f_a. For the other wavelengths, we use the function f_a calculate from the near infrared wavelength in Eq. (26) to calculate the contribution of the aerosol scattering due to the environment in the other bands.
(i) We applied this correction on the series of Balaton Lake images and Figure 5 shows the result of these corrections of the Fresnel scattering effect and the adjacency effects. For these spectra, we calculate the average water reflectance for all pixels classified inland waters from the geo localization. On this figure, the shape of the spectrum is almost the same for the visible part of the spectrum. For the near infrared part, we have two different trends. The first one is, for most of case, between 3 and 4 percent of water reflectance. The second one is around 8 percent for 3 days in the series of images. These 3 days corresponds to the 214, 216 and 223 Julian days where the sensor viewing gives geometric distortions. Actually, when the sensor zenith angle is around 60°, the geo localization can create a mistake of one or two pixels for the inland water mask and so consider some high value pixels like inland waters pixels and increase the

average reflectance. Figure 5, right, gives the spectra of the series of images after corrections of the Fresnel scattering effect and the molecular and aerosol scattering due to the environment. These corrections do not change the shape of the spectra but the variability seems to be high for the period cover by the series of images.

Fig. 5: Water reflectance for all SeaWiFS bands for the series of Balaton Lake images before Fresnel and environment corrections (a) and after corrections (b)

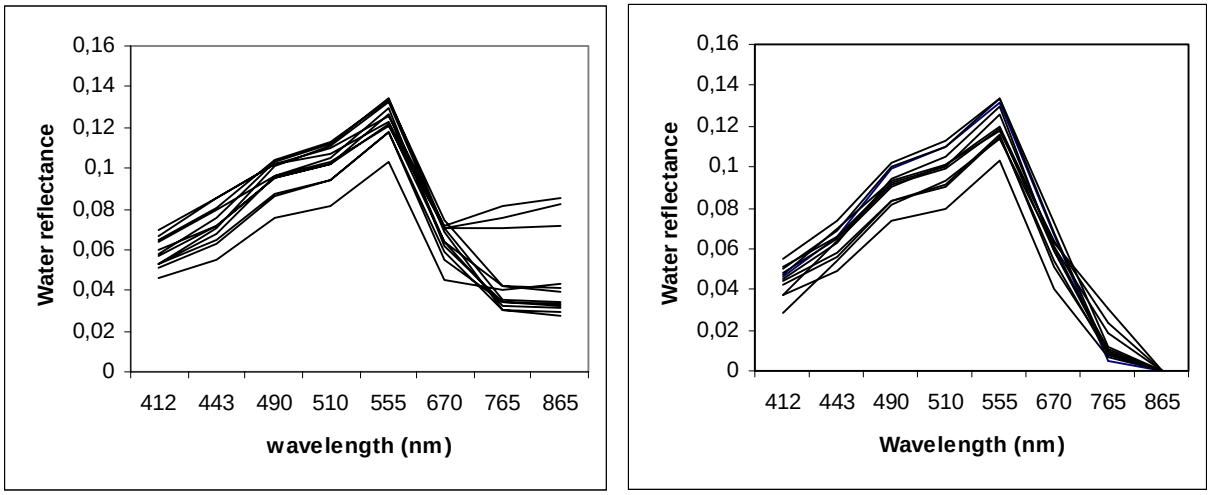

Figures 6 shows two distributions of water reflectance at 765 nm for two different days, with two different aerosols loading. We can see that before correction, the standard deviation of the distribution is higher when the aerosol loading is heavy. This is due to the adjacency effect of aerosols.

Fig. 6: Water reflectance distributions at 765 nm for different value of aerosol optical thickness. (a) for an aerosol optical thickness of 0.437 and (b) 0.089.

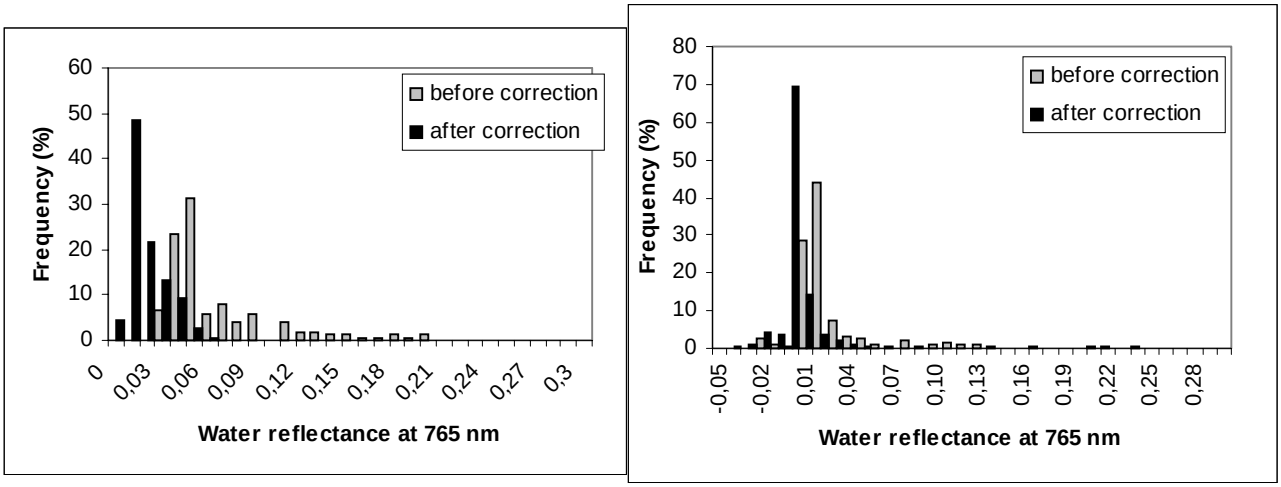

4. CONCLUSION

Standard algorithms for aerosol remote sensing over land are available to perform atmospheric corrections over inland waters. This algorithm uses spectral bands, which are present in «ocean colour» missions, and in principle, the

atmospheric correction can be achieved. Because of the higher reflectivity of the land, the water reflectance, retrieved after the standard atmospheric corrections, is contaminated by the so-called adjacency effects. At the edges of a lake (or for the full lake if it size is small), this effect has to be flagged. We give here some crude indications on a procedure devoted to remove these adjacency effects. The coupling between atmospheric scattering and Fresnel reflection has also to be corrected. This correction can be simply based assuming that the water should be dark at 865 nm and that the residual measured reflectance at 865 nm, which corresponds to this contribution, can be easily evaluated in the other spectral bands.

AKNOWLEDGEMENTS

Thanks to the DAAC at the GSFC for the production and the distribution of the Level 1A SeaWiFS images. This work was supported by the European Community in the Fifth Frame Work Program, IST, in the SISCAL project. We also thank D. Dessailly and O. Hars for their technical assistance.

REFERENCES

1. D. Antoine and A. Morel, "A multiple scattering algorithm for atmospheric correction of remotely sensed ocean colour (MERIS instrument) : principle and implementation for atmospheres carrying various aerosols including absorbing ones", *Int. J. Remote Sensing*. **20**, no 9. 1999.
2. H.R. Gordon, "Atmospheric correction of ocean color imagery in the Earth Observing System era", *Journal of Geophysical Research*. **102**, pp. 17081-17106, 1997.
3. B.N. Holben, T. F. Eck, I. Slutsker, D. Tanré, J. P. Buis, A. Setzer, E. Vermote, J. A. Reagan, Y. J. Kaufman, T. Nakajima, F. Lavenu, I. Jankowiak, and A. Smirnov, "AERONET- A Federated Instrument Network and Data Archive for Aerosol Characterization", *Remote Sens. Environ*. **66**: pp. 1-16, 1998.
4. C.E. Junge, "Air chemistry and radiochemistry", Academic Press, New York, 1963.
5. Y. J. Kaufman and C. Sendra, "Algorithm for automatic corrections to visible and near-infrared satellite imagery", *International Journal of Remote Sensing*. **9**, pp. 1357-1351, 1988.
6. Y. J Kaufman, D. Tanré, L. A. Remer, E. F.Vermote, A. Chu,and B. N. Holben, "Operational remote sensing of tropospheric aerosol over land from EOS moderate resolution imaging spectroradiometer", *Journal of Geophysical Research*. **102**, pp. 17051-17067, 1997.
7. Y.J. Kaufman and Tanré D., "Atmospherically resistant vegetation index (ARVI) for EOS-MODIS", *IEEE Trans. on Geosci. and Remote Sensing*. **30**, 2, 1992.
8. M. Leroy, V. Bruniquel-Pinel, O. Hautecoeur, F.M. Breon and F. Baret, « Corrections atmosphérique des données MERIS/ENVISAT : caractérisation de la BRDF de surfaces sombres », Rapport final ESTEC, 1998
9. A. I. Lyapustin and Y. J. Kaufman, "Role of adjacency effect in the remote sensing of aerosol", *Journal of Geophysical Research*. **106**, pp. 11909-11916, 2001.
10. D. Ramon and R. Santer, "Operational Remote Sensing of Aerosols over Land to Account for Directional Effects", *Applied Optics-LP*. **40** no 18, pp. 3060-3075, 2001.
11. R. Santer and C. Schmechtig, "Adjacency effects on water surfaces : primary scattering approximation and sensitivity study", *Applied Optics*. **39**, pp. 361-375, 2000.
12. R. Santer, V. Carrere, Ph. Dubuisson and J.C. Roger, "Atmospheric corrections over land for MERIS", *Int. J. Remote Sensing*.. **20** no 9, pp. 1819-1840, 1999.
13. C. Schmechtig, R. Borde, D. Ramon and R. Santer, "Validation of the atmospheric correction over land algorithm for the MOS sensor" *Proceedings of the 8th International Symposium Physical Measurements and Signatures in Remote Sensing*. 8-12 January, pp. 179-184, Aussois France, 2001.
14. C. J. Tucker, "Red and photographic infrared linear combinations for monitoring vegetation", *Remote Sensing of Environment*, **8**, pp. 127-150, 1979.
15. E.Vermote, D. Tanré, J.L. Deuze, M. Herman and J.J. Morcrette, "Second simulation of the satellite signal in the solar spectrum (6S), User's guide", 1995

.

*vidot@mren2.univ-littoral.fr; phone 33(0)3 21 99 64 15; fax 33(0)3 21 99 64 01; Université du Littoral Côte d'Opale, Maison de la Recherche en Environnment Naturel, 32 avenue Foch, 62930 Wimereux, France ; **santer@mren2.univ-littoral.fr phone 33(0)3 21 99 64 26; fax 33(0)3 21 99 64 01; Université du Littoral Côte d'Opale, Maison de la Recherche en Environnment Naturel, 32 avenue Foch, 62930 Wimereux, France